Comparing symmetry restoration in the QCD-like three quark flavor models

Vivek Kumar Tiwari*

Department of Physics, University of Allahabad, Allahabad 211002, India.

(Dated: January 17, 2013)

We are computing the modifications for the scalar and pseudoscalar meson masses and mixing angles due to the proper accounting of fermionic vacuum fluctuation in the framework of generalized $2+1$ flavor quark-meson model and Polyakov loop augmented Quark Meson model (PQM). The renormalized contribution of the divergent fermionic vacuum fluctuation at one loop level, makes these models effective quantum chromodynamics (QCD)-like models. It has been explicitly shown that analytical expressions for the model parameters, meson masses and mixing angles, do not depend on any arbitrary renormalization scale. We have investigated how the incorporation of fermionic vacuum fluctuation in quark meson and PQM models qualitatively and quantitatively affects the convergence in the masses of the chiral partners in pseudoscalar (π, η, η', K) and scalar (σ, a_0, f_0, κ) meson nonets as the temperature is varied on the reduced temperature scale. Chiral symmetry restoration trends emerging from the temperature variations of the meson masses of the chiral partners and mixing angles, have been identified and compared with in different model scenarios. Comparison of present results in the quark meson model with vacuum term (QMVT) and PQM model with vacuum term (PQMVT) with the already existing calculations in the bare $2+1$ quark meson and PQM models, show that the restoration of chiral symmetry becomes smoother due to the influence of the fermionic vacuum term. We find that the melting of the strange condensate registers a significant increase in the presence of fermionic vacuum term and its highest melting is found in PQMVT model. The role of $U_A(1)$ anomaly in determining the isoscalar masses and mixing angles for the pseudoscalar (η and η') and scalar (σ and f_0) meson complex, has also been significantly modified due to the presence of fermionic vacuum term. The interplay of chiral symmetry restoration effects and the setting up of $U_A(1)$ restoration trends has been shown to be significantly modified by the incorporation of fermionic vacuum fluctuation in the effective potential of the quark meson and PQM models.

PACS numbers: 12.38.Aw, 11.30.Rd, 12.39.Fe, 11.10.Wx

I. INTRODUCTION

The strong interaction theory predicts that normal hadronic matter goes through a phase transition and produces a collective form of matter known as the Quark Gluon Plasma (QGP) under the extreme conditions of high temperature and/or density when the individual hadrons dissolve into their quark and gluon constituents [1–4]. Relativistic heavy ion collision experiments at RHIC (BNL), LHC (CERN) and the future CBM experiments at the FAIR facility (GSI-Darmstadt) aim to create and study such a collective state of matter. Study of the different aspects of this phase transition, is a tough and challenging task because Quantum Chromodynamics (QCD) which is the theory of strong interaction, becomes nonperturbative in the low energy limit. However the QCD vacuum reveals itself through the process of spontaneous chiral symmetry breaking and phenomenon of color confinement.

In the zero quark mass limit, chiral condensate works as an order parameter for the spontaneous breakdown of the chiral symmetry in the low energy hadronic vacuum of the QCD. For the infinitely heavy quarks, in the pure gauge $SU_c(3)$ QCD, the $Z(3)$ (Center symmetry of the QCD color gauge group) symmetry, which is the symmetry of hadronic vacuum, gets spontaneously broken in the high temperature/density regime of QGP. Here the expectation value of the Wilson line (Polyakov loop) is related to the free energy of a static color charge, hence it serves as the order parameter of the confinement-deconfinement phase transition [5]. Even though the center symmetry is always broken with the inclusion of dynamical quarks in the system, one can regard the Polyakov loop as an approximate order parameter because it is a good indicator of the confinement-deconfinement transition [6, 7].

The lattice QCD calculations (see e.g. [8–16]) give us important information and insights regarding various aspects of the transition, like the restoration of chiral symmetry in QCD, order of the confinement-deconfinement phase transition, richness of the QCD phase structure and mapping of the phase diagram. Since lattice calculations are technically involved and various issues are not conclusively settled within the lattice community, one resorts to the calculations within the ambit of phenomenological models [17–26] developed in terms of effective degrees of freedom. These model investigations complement the lattice simulation studies and give much needed insight about the regions of phase diagram inaccessible to lattice

*Electronic address: vivekkrt@gmail.com

simulations. Lot of current effective model building activity, is centered around combining the features of spontaneous breakdown of both chiral symmetry as well as the center $Z(3)$ symmetry of QCD in one single model (see for example [27–49]). In these models chiral condensate and Polyakov loop are simultaneously coupled to the quark degrees of freedom.

The behavior patterns of mesons and their properties in the hot and dense medium, have been investigated in the several two and three flavor NJL, PNJL models (e.g. [50–54]) and also in the $SU(2)$ version of linear sigma model (e.g. [55–57]). Since the parity doubling of mesons signals the restoration of chiral symmetry, these studies look for the emergence of mass convergence patterns in the masses of the chiral partners in pseudoscalar (π, η, η', K) and scalar mesons (σ, a_0, f_0, κ). We know that the basic QCD lagrangian has the global $SU_{R+L}(3) \times SU_{R-L}(3) \times U_A(1)$ symmetry. For the $SU(3)$ Linear Sigma Model, several explicit as well as spontaneous symmetry breaking patterns of $SU_V(3) \times SU_A(3)$, have been discussed by Lenaghan et al.in Ref.[58]. Enlarging the Linear Sigma Model with the inclusion of quarks [59] in the 2+1 flavor breaking scenario, Schaefer et al. studied the consequences of $SU(3)$ chiral symmetry restoration for scalar and pseudoscalar meson masses and mixing angles, in the presence as well as the absence of $U_A(1)$ axial symmetry, as the temperature is increased through the phase transition temperature. It was shown by 't Hooft [60] that the $U_A(1)$ axial symmetry does not exist at the quantum level and the instanton effects explicitly break it to $Z_A(N_f)$. Due to the $U_A(1)$ anomaly, the η' meson does not remain massless Goldstone boson in the chiral limit of zero quark masses and it acquires a mass of about 1 GeV. This happens due to the flavor mixing, a phenomenon that lifts the degeneracy between the π and η' which otherwise would have been degenerate with π in $U(3)$ even if the explicit chiral symmetry breaking is present. There is large violation in Okubo-Zweig-Iizuka (OZI) rule for both pseudoscalar and scalar mesons and ideal mixing is not achieved because of strong flavor mixing between nonstrange and strange flavor components of the mesons [53]. Hence $U_A(1)$ restoration will have important observable effects on scalar and pseudoscalar meson masses as well as the mixing angles.

The effect of Polyakov loop potential on the behavior of meson masses and mixing angles has been studied by Costa et. al in the PNJL model [53] and by Contrera et.al in the nonlocal PNJL model [54]. Here in the NJL model based studies, mesons are generated by some prescription [52] and the η' is not a well defined quantity [61]. It becomes unbound soon after the temperature is raised from zero. In the 2+1 flavor quark meson linear sigma model investigations by Schaefer et al. [59, 62], the mesons are the explicit degrees of freedom included in the lagrangian from the very outset and the $U_A(1)$ breaking 't Hooft coupling term is constant. Recently, we investigated the influence of the Polyakov loop potential on the meson mass and mixing angle calculations in the scalar and pseudoscalar sector, in the framework of generalized 2+1 flavor quark meson model enlarged with the inclusion of Polyakov loop [28, 63–65].

The chiral symmetry breaking mechanism in the QM/PQM model is different from that of the NJL/PNJL model. In the NJL/PNJL model, the fermionic vacuum fluctuation leads to the dynamical breaking of the chiral symmetry. While in most of the QM/PQM model calculations, fermionic vacuum loop contribution to the grand potential got frequently neglected till recently [24, 31, 55, 56, 59] because here, the spontaneous breaking of chiral symmetry is generated by the mesonic potential itself. Recently, Skokov et. al. incorporated the appropriately renormalized fermionic vacuum fluctuation [66] in the thermodynamic potential of the two flavor QM model which becomes an effective QCD-like model because now it can reproduce the second order chiral phase transition at $\mu = 0$ as expected from the universality arguments [17] for the two massless flavors of QCD. The fermionic vacuum correction and its influence has also been investigated in earlier works [67–70]. In a recent work [71], we generalized the proper accounting of renormalized fermionic vacuum fluctuation in the two flavor PQM model to the non-zero chemical potentials and found that the position of critical end point shifts to a significantly higher chemical potential in the μ and T plane of the phase diagram. Very recently, Schaefer et. al.[72] estimated the size of critical region around the CEP in a three flavor PQM model in the presence of the fermionic vacuum term. Sandeep et al. also investigated the phase structure and made comparisons with lattice data in another recent 2+1 quark flavor study with the effect of fermionic vacuum term [73]. In a very recent work [74], the present author explored and compared the details of criticality in the two flavor QM, PQM models in the presence and absence of fermionic vacuum correction.

In the present work, the author will explore how the proper accounting fermionic vacuum correction in the QM and PQM models, qualitatively and quantitatively affects the convergence of the masses of chiral partners, when the parity doubling takes place as the temperature is increased through T_c and the partial restoration of chiral symmetry is achieved. We will also be studying the effect of fermionic vacuum correction on the interplay of $SU_A(3)$ chiral symmetry and $U_A(1)$ symmetry restoration in the presence as well as absence of Polyakov loop potential in QM model. Since we are lacking in the experimental information on the behavior of mass and mixing angle observables in the medium, a comparative study of these quantities in different model scenarios and circumstances becomes all the more desirable.

The arrangement of this paper is as follows. In Sec.II we recapitulate the formulation of the model. The description of grand potential in the mean field approach has been presented in Sec. III. We have derived the modification of meson masses due to the

fermionic vacuum correction and presented the scale independent calculation of the effective potential with the renormalized model parameters in Sec.IV where the formulae for meson masses and mixing angles have also been discussed. In Sec.V, we will be discussing the numerical results and plots for understanding and analyzing the effect of fermionic vacuum correction on the chiral symmetry restoration. Summary and conclusion is presented in the last Sec.VI.

II. MODEL FORMULATION

We will be working in the generalized three flavor Quark Meson Chiral Linear Sigma Model which has been combined with the Polyakov loop potential [28, 63–65]. In this model, quarks coming in three flavor are coupled to the $SU_V(3) \times SU_A(3)$ symmetric mesonic fields together with spatially constant temporal gauge field represented by Polyakov loop potential. Polyakov loop field $\Phi(\vec{x})$ is defined as the thermal expectation value of color trace of Wilson loop in temporal direction

$$\Phi = \frac{1}{N_c}\mathrm{Tr}_c L, \qquad \Phi^* = \frac{1}{N_c}\mathrm{Tr}_c L^\dagger \tag{1}$$

where L(x) is a matrix in the fundamental representation of the $SU_c(3)$ color gauge group.

$$L(\vec{x}) = \mathcal{P}\mathrm{exp}\left[i\int_0^\beta d\tau A_0(\vec{x},\tau)\right] \tag{2}$$

Here $\mathcal{P}$ is path ordering, A_0 is the temporal vector field and $\beta = T^{-1}$ [5].

The model Lagrangian is written in terms of quarks, mesons, couplings and Polyakov loop potential $\mathcal{U}(\Phi, \Phi^*, T)$.

$$\mathcal{L}_{PQM} = \mathcal{L}_{QM} - \mathcal{U}\big(\Phi, \Phi^*, T\big) \tag{3}$$

where the Lagrangian in Quark Meson Chiral Sigma model

$$\mathcal{L}_{QM} = \bar{q_f}\big(i\gamma^\mu D_\mu - g\, T_a\big(\sigma_a + i\gamma_5\pi_a\big)\big)q_f + \mathcal{L}_m \tag{4}$$

The coupling of quarks with the uniform temporal background gauge field is effected by the following replacement $D_\mu = \partial_\mu - iA_\mu$ and $A_\mu = \delta_{\mu 0}A_0$ (Polyakov gauge), where $A_\mu = g_s A_\mu^a \lambda^a/2$. g_s is the $SU_c(3)$ gauge coupling. λ_a are Gell-Mann matrices in the color space, a runs from $1 \cdots 8$. $q_f = (u, d, s)^T$ denotes the quarks coming in three flavors and three colors. g is the flavor blind Yukawa coupling that couples the three flavor of quarks with nine mesons in the scalar ($\sigma_a, J^P = 0^+$) and pseudoscalar ($\pi_a, J^P = 0^-$) sectors.

The quarks have no intrinsic mass but become massive after spontaneous chiral symmetry breaking because of non vanishing vacuum expectation value of the chiral condensate. The mesonic part of the lagrangian has the following form

$$\begin{aligned}\mathcal{L}_m \;=\; & \mathrm{Tr}\left(\partial_\mu M^\dagger \partial^\mu M\right) - m^2\mathrm{Tr}(M^\dagger M) - \lambda_1\left[\mathrm{Tr}(M^\dagger M)\right]^2 \\ & -\lambda_2\mathrm{Tr}\left(M^\dagger M\right)^2 + c\big[det(M) + det(M^\dagger)\big] \\ & +\mathrm{Tr}\left[H(M + M^\dagger)\right].\end{aligned} \tag{5}$$

The chiral field M is a 3×3 complex matrix comprising of the nine scalars σ_a and the nine pseudoscalar π_a mesons.

$$M = T_a\xi_a = T_a(\sigma_a + i\pi_a) \tag{6}$$

Here T_a represent 9 generators of $U(3)$ with $T_a = \frac{\lambda_a}{2}$. $a = 0, 1 \ldots 8$. λ_a are standard Gell-Mann matrices with $\lambda_0 = \sqrt{\frac{2}{3}}\,\mathbf{1}$. The generators follow $U(3)$ algebra $[T_a, T_b] = if_{abc}T_c$ and $\{T_a, T_b\} = d_{abc}T_c$ where f_{abc} and d_{abc} are standard antisymmetric and symmetric structure constants respectively with $f_{ab0} = 0$ and $d_{ab0} = \sqrt{\frac{2}{3}}\,\mathbf{1}\,\delta_{\mathbf{ab}}$ and matrices are normalized as $\mathrm{Tr}(T_aT_b) = \frac{\delta_{ab}}{2}$.

The $SU_L(3) \times SU_R(3)$ chiral symmetry is explicitly broken by the explicit symmetry breaking term

$$H = T_a h_a \tag{7}$$

Here H is a 3×3 matrix with nine external parameters. The ξ field picks up the nonzero vacuum expectation value, $\bar{\xi}$ due to the spontaneous breakdown of the chiral symmetry. Since $\bar{\xi}$ must have the quantum numbers of the vacuum, explicit breakdown of the chiral symmetry is only possible with three nonzero parameters h_0, h_3 and h_8. We are neglecting isospin symmetry breaking hence we choose $h_0,\ h_8 \neq 0$. This leads to the $2 + 1$ flavor symmetry breaking scenario with nonzero condensates $\bar{\sigma_0}$ and $\bar{\sigma_8}$.

Apart from h_0 and h_8, the other parameters in the model are five in number. These are the squared tree-level mass of the meson fields m^2, quartic coupling constants λ_1 and λ_2, a Yukawa coupling g and a cubic coupling constant c which models the $U_A(1)$ axial anomaly of the QCD vacuum.

Since it is broken by the quantum effects, the $U_A(1)$ axial which otherwise is a symmetry of the classical lagrangian, becomes anomalous [75] and gives large mass to η' meson ($m_{\eta'} = 940$ MeV). In the absence of $U_A(1)$ anomaly, η' meson would have been the ninth pseudoscalar Goldstone boson, resulting due to the spontaneous break down of the chiral $U_A(3)$ symmetry. The entire pseudoscalar nonet corresponding to spontaneously broken $U_A(3)$, would consist of the three π, four K, η and η' mesons, which are the massless pure Goldstone modes when $H = 0$ and they become pseudo Goldstone modes after acquiring finite mass due to nonzero H in different symmetry breaking scenarios. The particles coming from octet (a_0, f_0, κ) and singlet (σ) representations of $SU_V(3)$ group, constitute scalar nonet (σ, a_0, f_0, κ). In order to study the chiral symmetry restoration at high temperatures, we will be

investigating the trend of convergence in the masses of chiral partners occurring in pseudoscalar (π, η, η', K) and scalar (σ, a_0, f_0, κ) nonets, in the $2+1$ flavor symmetry breaking scenario.

A. Polyakov loop potential

The effective potential $\mathcal{U}(\Phi, \Phi^*, T)$ is constructed such that it reproduces thermodynamics of pure glue theory on the lattice for temperatures upto about twice the deconfinement phase transition temperature. In this work, we are using logarithmic form of Polyakov loop effective potential [34]. The results produced by this potential are known to be fitted well to the lattice results. This potential is given by the following expression

$$\frac{\mathcal{U}_{\log}(\Phi, \Phi^*, T)}{T^4} = -\frac{a(T)}{2}\Phi^*\Phi + b(T)\ln[1 - 6\Phi^*\Phi + 4(\Phi^{*3} + \Phi^3) - 3(\Phi^*\Phi)^2] \quad (8)$$

where the temperature dependent coefficients are as follow

$$a(T) = a_0 + a_1\left(\frac{T_0}{T}\right) + a_2\left(\frac{T_0}{T}\right)^2 \quad b(T) = b_3\left(\frac{T_0}{T}\right)^3 .$$

The parameters of Eq.(8) are

$$a_0 = 3.51\ , \qquad a_1 = -2.47\ ,$$
$$a_2 = 15.2\ , \qquad b_3 = -1.75$$

The critical temperature for deconfinement phase transition $T_0 = 270$ MeV is fixed for pure gauge Yang Mills theory. In the presence of dynamical quarks T_0 is directly linked to the mass-scale $\Lambda_{\rm QCD}$, the parameter which has a flavor and chemical potential dependence in full dynamical QCD and $T_0 \to T_0(N_f, \mu)$ [27, 29].

III. GRAND POTENTIAL IN THE MEAN FIELD APPROACH

We are considering a spatially uniform system in thermal equilibrium at finite temperature T and quark chemical potential $\mu_f (f = u, d, s)$. The partition function is written as the path integral over quark/antiquark and meson fields [28, 59]

$$\mathcal{Z} = \mathrm{Tr}\exp[-\beta(\hat{\mathcal{H}} - \sum_{f=u,d,s}\mu_f\hat{\mathcal{N}_f})] = \int\prod_a \mathcal{D}\sigma_a\mathcal{D}\pi_a\int\mathcal{D}q\mathcal{D}\bar{q}\exp\Big[-\int_0^\beta d\tau\int_V d^3x \Big(\mathcal{L}^{\mathcal{E}}_{\mathcal{QMS}} + \sum_{f=u,d,s}\mu_f\bar{q}_f\gamma^0 q_f\Big)\Big]. \quad (9)$$

where V is the three dimensional volume of the system, and $\beta = \frac{1}{T}$. For three quark flavors, in general, the three quark chemical potentials are different. In this work, we assume that $SU_V(2)$ symmetry is preserved and neglect the small difference in masses of u and d quarks. Thus the quark chemical potential for the u and d quarks become equal $\mu_x = \mu_u = \mu_d$. The strange quark chemical potential is $\mu_y = \mu_s$. Further we consider symmetric quark matter and net baryon number to be zero.

Here, the partition function is evaluated in the mean-field approximation[28, 56, 59, 62]. We replace meson fields by their expectation values $\langle\Phi\rangle = T_0\bar{\sigma_0} + T_8\bar{\sigma_8}$ and neglect both thermal as well as quantum fluctuations of meson fields while quarks and antiquarks are retained as quantum fields. Now following the standard procedure as given in Refs. [27, 33, 43, 76] one can obtain the expression of grand potential as sum of pure gauge field contribution $\mathcal{U}(\Phi, \Phi^*, T)$, meson contribution and quark/antiquark contribution evaluated in the presence of Polyakov loop,

$$\Omega_{\rm MF}(T,\mu) = -\frac{T\ln Z}{V} = U(\sigma_0, \sigma_8) + \mathcal{U}(\Phi, \Phi^*, T) + \Omega_{\bar{q}q}(T,\mu) \quad (10)$$

In order to study $2+1$ flavor case, one performs following basis transformation of condensates and external fields from original singlet octet (0, 8) basis to nonstrange strange basis (x, y).

$$\sigma_x = \sqrt{\frac{2}{3}}\bar{\sigma}_0 + \frac{1}{\sqrt{3}}\bar{\sigma}_8, \quad (11)$$

$$\sigma_y = \frac{1}{\sqrt{3}}\bar{\sigma}_0 - \sqrt{\frac{2}{3}}\bar{\sigma}_8. \quad (12)$$

Similar expressions exist for writing the external fields (h_x, h_y) in terms of (h_0, h_8). Thus the nonstrange and strange quark/antiquark decouple and the quark masses become

$$m_x = g\frac{\sigma_x}{2}, \qquad m_y = g\frac{\sigma_y}{\sqrt{2}} \quad (13)$$

Quarks become massive in symmetry broken phase because of non zero vacuum expectation values of the condensates.

The mesonic potential in the nonstrange-strange basis reads,

$$U(\sigma_x, \sigma_y) = \frac{m^2}{2}\left(\sigma_x^2 + \sigma_y^2\right) - h_x\sigma_x - h_y\sigma_y - \frac{c}{2\sqrt{2}}\sigma_x^2\sigma_y + \frac{\lambda_1}{2}\sigma_x^2\sigma_y^2 + \frac{1}{8}\left(2\lambda_1 + \lambda_2\right)\sigma_x^4 + \frac{1}{8}\left(2\lambda_1 + 2\lambda_2\right)\sigma_y^4\ , \quad (14)$$

The quark/antiquark Polyakov loop contribution is

	Meson masses for Scalars and Pseudoscalars $\eta', \eta, \eta_{NS}, \eta_S$		Pseudoscalar Meson masses
$m^2_{a_0}$	$m^2+\lambda_1(x^2+y^2)+\frac{3\left(\lambda_{2\mathrm{v}}-\delta m_x-\frac{4n}{3}\right)}{2}x^2+\frac{\sqrt{2}c}{2}y$	m^2_π	$m^2+\lambda_1(x^2+y^2)+\frac{(\lambda_{2\mathrm{v}}-\delta m_x)}{2}x^2-\frac{\sqrt{2}c}{2}y$
m^2_κ	$\lambda_1(x^2+y^2)+\frac{(\lambda_{2\mathrm{v}}-\delta m_x)}{2}(x^2+\sqrt{2}xy+2y^2)$	m^2_K	$\lambda_1(x^2+y^2)+\frac{(\lambda_{2\mathrm{v}}-\delta m_x)}{2}(x^2-\sqrt{2}xy+2y^2)$
	$+m^2+\frac{c}{2}x+\delta m_k-$		$+m^2-\frac{c}{2}x-\delta m_k+$
$m^2_{s,00}$	$\frac{\lambda_1}{3}(7x^2+4\sqrt{2}xy+5y^2)+\left(\lambda_{2\mathrm{v}}-\frac{4n}{3}\right)(x^2+y^2)$	$m^2_{p,00}$	$\lambda_1(x^2+y^2)+\frac{\lambda_{2\mathrm{v}}}{3}(x^2+y^2)+\frac{c}{3}(2x+\sqrt{2}y)$
	$+m^2-\frac{\sqrt{2}c}{3}(\sqrt{2}x+y)-(x^2\delta m_x+y^2\delta m_y)$		$+m^2-\frac{1}{3}(x^2\delta m_x+y^2\delta m_y)$
$m^2_{s,88}$	$\frac{\lambda_1}{3}(5x^2-4\sqrt{2}xy+7y^2)+\left(\lambda_{2\mathrm{v}}-\frac{4n}{3}\right)(\frac{x^2}{2}+2y^2)$	$m^2_{p,88}$	$\lambda_1(x^2+y^2)+\frac{\lambda_{2\mathrm{v}}}{6}(x^2+4y^2)-\frac{c}{6}(4x-\sqrt{2}y)$
	$+m^2+\frac{\sqrt{2}c}{3}(\sqrt{2}x-\frac{y}{2})-(\frac{x^2}{2}\delta m_x+2y^2\delta m_y)$		$+m^2-\frac{1}{6}(x^2\delta m_x+4y^2\delta m_y)$
$m^2_{s,08}$	$\frac{2\lambda_1}{3}(\sqrt{2}x^2-xy-\sqrt{2}y^2)+\sqrt{2}\left(\lambda_{2\mathrm{v}}-\frac{4n}{3}\right)(\frac{x^2}{2}-y^2)$	$m^2_{p,08}$	$\frac{\sqrt{2}\lambda_{2\mathrm{v}}}{6}(x^2-2y^2)-\frac{c}{6}(\sqrt{2}x-2y)$
	$+\frac{c}{3\sqrt{2}}(x-\sqrt{2}y)-\sqrt{2}(\frac{x^2}{2}\delta m_x-y^2\delta m_y)$		$-\frac{\sqrt{2}}{6}(x^2\delta m_x-2y^2\delta m_y)$
$m^2_{\sigma(\eta')}$	$m^2_{s(p),00}\cos^2\theta_{s(p)}+m^2_{s(p),88}\sin^2\theta_{s(p)}+2m^2_{s(p),08}\sin\theta_{s(p)}\cos\theta_{s(p)}$	$m^{\mathrm{m}\,2}_\pi$	$m^2+\lambda_1(x^2+y^2)+\frac{\lambda_2}{2}x^2-\frac{\sqrt{2}c}{2}y$
$m^2_{f_0(\eta)}$	$m^2_{s(p),00}\sin^2\theta_{s(p)}+m^2_{s(p),88}\cos^2\theta_{s(p)}-2m^2_{s(p),08}\sin\theta_{s(p)}\cos\theta_{s(p)}$	$m^{\mathrm{m}\,2}_K$	$m^2+\lambda_1(x^2+y^2)+\frac{\lambda_2}{2}(x^2-\sqrt{2}xy+2y^2)-\frac{c}{2}x$
$m^2_{\sigma(\eta)_{NS}}$	$\frac{1}{3}(2m^2_{s(p),00}+m^2_{s(p),88}+2\sqrt{2}m^2_{s(p),08})$	${m^{\mathrm{m}}_{p,00}}^2$	$m^2+\lambda_1(x^2+y^2)+\frac{\lambda_2}{3}(x^2+y^2)+\frac{c}{3}(2x+\sqrt{2}y)$
$m^2_{\sigma(\eta)_S}$	$\frac{1}{3}(m^2_{s(p),00}+2m^2_{s(p),88}-2\sqrt{2}m^2_{s(p),08})$	${m^{\mathrm{m}}_{p,88}}^2$	$m^2+\lambda_1(x^2+y^2)+\frac{\lambda_2}{6}(x^2+4y^2)-\frac{2c}{3}x+\frac{\sqrt{2}c}{6}y$

TABLE I: The squared masses of scalar and pseudoscalar mesons appear in nonstrange strange basis.In this table $x=\sigma_x$, $y=\sigma_y$, $\lambda_{2\mathrm{v}}=\lambda_{2s}+\lambda_{2+}$, $n=\frac{N_c g^4}{32\pi^2}$, $\delta m_x=4n\log\left(\frac{x}{(2f_K-f_\pi)}\right)$, $\delta m_y=4n\log\left(\frac{\sqrt{2}\ y}{(2f_K-f_\pi)}\right)$ and $\delta m_k\pm=\frac{4\sqrt{2}\ ny^3}{(x\pm\sqrt{2}y)}\log\left(\frac{\sqrt{2}y}{x}\right)$. The masses of nonstrange $\sigma_{NS}(\eta_{NS})$, strange $\sigma_S(\eta_S)$ mesons are given in the last two rows of second column.

Model	c[MeV]	$m^2\ [MeV^2]$	λ_1	λ_{2s}	$h_x\ [MeV^3]$	$h_y\ [MeV^3]$
QM W/$U_A(1)$	4807.84	$(342.52)^2$	1.40	46.48	$(120.73)^3$	$(336.41)^3$
QMVT W/$U_A(1)$	4807.84	$-(184.86)^2$	-1.689	46.48	$(120.73)^3$	$(336.41)^3$
QM W/o$U_A(1)$	0	$-(189.85)^2$	-17.01	82.47	$(120.73)^3$	$(336.41)^3$
QMVT W/o$U_A(1)$	0	$-(424.68)^2$	-20.46	82.47	$(120.73)^3$	$(336.41)^3$

TABLE II: parameters for $m_\sigma=600$ MeV with and without $U_A(1)$ axial anomaly term.

written as,

$$\begin{aligned}\Omega_{\bar{q}q}(T,\mu) = &\quad \Omega^{\mathrm{vac}}_{q\bar{q}}+\Omega^{\mathrm{T}}_{q\bar{q}}\\ = &\quad -2N_f\int\frac{d^3p}{(2\pi)^3}\{N_cE_q\theta(\Lambda^2-\vec{p}^2)\\ &\quad +T[\ln g^+_f+\ln g^-_f]\}\end{aligned}\tag{15}$$

The first term of the Eq. (15) is the renormalized fermionic vacuum loop contribution. As evaluated in Ref.[66, 71], it is given by

$$\Omega^{\mathrm{vac}}_{q\bar{q}}=-\frac{N_cN_f}{8\pi^2}m_f^4\ln\left(\frac{m_f}{M}\right).\tag{16}$$

Here M denotes an arbitrary renormalization scale. In the second term g^+_f and g^-_f are defined after taking trace over color space

$$g^+_f=\left[1+3\Phi e^{-E^+_f/T}+3\Phi^* e^{-2E^+_f/T}+e^{-3E^+_f/T}\right]\tag{17}$$

$$g^-_f=\left[1+3\Phi^* e^{-E^-_f/T}+3\Phi e^{-2E^-_f/T}+e^{-3E^-_f/T}\right]\tag{18}$$

$\mathrm{E}^\pm_f=E_f\mp\mu$ and E_f is the flavor dependent single particle energy of quark/antiquark.

$$E_f=\sqrt{p^2+{m_f}^2}\tag{19}$$

m_f is the flavor dependent quark mass.

IV. MESON MASSES, RENORMALIZED MODEL PARAMETERS AND MIXING ANGLES

In the effective potential Eq.(10), the pure mesonic potential U(σ_x,σ_y) and the renormalized fermionic vacuum term are relevant for fixing the vacuum ($T=$

	$m^2_{x,a}m^2_{x,b}/g^4$	$m^2_{x,ab}/g^2$	$m^2_{y,a}m^2_{y,b}/g^4$	$m^2_{y,ab}/g^2$
$\sigma_0\ \sigma_0$	$\frac{1}{3}\sigma_x^2$	$\frac{2}{3}$	$\frac{1}{3}\sigma_y^2$	$\frac{1}{3}$
$\sigma_1\ \sigma_1$	$\frac{1}{2}\sigma_x^2$	1	0	0
$\sigma_4\ \sigma_4$	0	$\sigma_x\frac{\sigma_x+\sqrt{2}\sigma_y}{\sigma_x^2-2\sigma_y^2}$	0	$\sigma_y\frac{\sqrt{2}\sigma_x+2\sigma_y}{2\sigma_y^2-\sigma_x^2}$
$\sigma_8\ \sigma_8$	$\frac{1}{6}\sigma_x^2$	$\frac{1}{3}$	$\frac{2}{3}\sigma_y^2$	$\frac{2}{3}$
$\sigma_0\ \sigma_8$	$\frac{\sqrt{2}}{6}\sigma_x^2$	$\frac{\sqrt{2}}{3}$	$-\frac{\sqrt{2}}{3}\sigma_y^2$	$-\frac{\sqrt{2}}{3}$
$\pi_0\ \pi_0$	0	$\frac{2}{3}$	0	$\frac{1}{3}$
$\pi_1\ \pi_1$	0	1	0	0
$\pi_4\ \pi_4$	0	$\sigma_x\frac{\sigma_x-\sqrt{2}\sigma_y}{\sigma_x^2-2\sigma_y^2}$	0	$\sigma_y\frac{\sqrt{2}\sigma_x-2\sigma_y}{\sigma_x^2-2\sigma_y^2}$
$\pi_8\ \pi_8$	0	$\frac{1}{3}$	0	$\frac{2}{3}$
$\pi_0\ \pi_8$	0	$\frac{\sqrt{2}}{3}$	0	$-\frac{\sqrt{2}}{3}$

TABLE III: First and second derivative of squared quark mass in nonstrange-strange basis with respect to meson fields are evaluated at minimum. Sum over two light flavors, denoted by symbol x, is in third and fourth column. The last two columns have only strange quark mass flavor denoted by symbol y.

$0, \mu = 0)$ parameters m^2, λ_1, λ_2 and c. We write

$$\Omega(\sigma_x, \sigma_y) = \Omega^{\rm vac}_{q\bar{q}} + U(\sigma_x, \sigma_y) \tag{20}$$

The curvature of the grand potential in Eq.(10) at the global minimum gives scalar and pseudoscalar meson masses.

$$m^2_{\alpha,ab} = \frac{\partial^2 \Omega_{\rm MF}(\sigma_x, \sigma_y, T, \mu)}{\partial \xi_{\alpha,a} \partial \xi_{\alpha,b}}\bigg|_{min} \tag{21}$$

here subscript $\alpha =$ s, p; s stands for scalar and p stands for pseudoscalar meson and a, $b = 0 \cdots 8$. We note that the Polyakov loop decouples from the mesonic sector at T=0 and the curvature of the grand potential reduces to the second derivative of $\Omega(\sigma_x, \sigma_y)$ in Eq. (20). In the PQMVT model, the meson mass modifications due to the fermionic vacuum contribution of the Dirac sea of quarks/antiquarks will be given by

$$\begin{aligned}
{\delta m^{\rm v}_{\alpha,ab}}^2 &= \frac{\partial^2 \Omega^{\rm vac}_{q\bar{q}}}{\partial \xi_{\alpha,a} \partial \xi_{\alpha,b}}\bigg|_{min} \\
&= -\frac{N_c}{8\pi^2} \sum_f \Big[\left(2 \log\left(\frac{m_f}{M}\right) + \frac{3}{2} \right) \left(\frac{\partial m_f^2}{\partial \xi_{\alpha,a}} \right) \left(\frac{\partial m_f^2}{\partial \xi_{\alpha,b}} \right) \\
&+ \left(\frac{m_f^2}{2} + 2 m_f^2 \log\left(\frac{m_f}{M}\right) \right) \frac{\partial^2 m_f^2}{\partial \xi_{\alpha,a} \partial \xi_{\alpha,b}} \Big]
\end{aligned} \tag{22}$$

We write $m^2_{f,a} \equiv \partial m_f^2 / \partial \xi_{\alpha,a}$ as the first partial derivative and $m^2_{f,ab} \equiv \partial m^2_{f,a} / \partial \xi_{\alpha,b}$ as the second partial derivative of the squared quark mass with respect to the meson fields $\xi_{\alpha,b}$. These derivatives as originally evaluated in [59] are given in Table III. The expressions for the vacuum meson masses and mixing angles which result purely from the second derivative of the mesonic potential U(σ_x, σ_x, T, μ) are given in Table II of Ref. [28] with their details discussed in Ref. [58, 59]. In the present calculation the vacuum masses that determine λ_2 and c are $m^2_\pi = {m^{\rm m}_\pi}^2 + {\delta m^{\rm v}_{p,11}}^2$, $m^2_K = {m^{\rm m}_K}^2 + {\delta m^{\rm v}_{p,44}}^2$, $m^2_{p,00} = {m^{\rm m}_{p,00}}^2 + {\delta m^{\rm v}_{p,00}}^2$ and $m^2_{p,88} = {m^{\rm m}_{p,88}}^2 + {\delta m^{\rm v}_{p,00}}^2$. We know that ${m^{\rm m}_\eta}^2 + {m^{\rm m}_{\eta'}}^2 = {m^{\rm m}_{p,00}}^2 + {m^{\rm m}_{p,88}}^2$. The superscript m denotes the pure mesonic potential contributions to the pseudoscalar meson masses. We have collected the expressions of these masses in the last four rows of the third and fourth column of Table II. After evaluating the mass modifications ${\delta m^{\rm v}_{p,ab}}^2$ due to the influence of fermionic vacuum for a,b=0,1,4 and 8, we give a brief description of the evaluation of the parameters λ_2 and c in the following.

$$\begin{aligned}
{m^{\rm m}_K}^2 = m^2_K + \frac{N_c g^4}{64\pi^2} \left(\frac{x - \sqrt{2}y}{x^2 - 2y^2} \right) \left(x^3 X + 2\sqrt{2} y^3 Y \right) \ ; \ {m^{\rm m}_\pi}^2 = m^2_\pi + \frac{N_c g^4}{64\pi^2} x^2 X \ with \ x = \sigma_x, y = \sigma_y \\
\left({m^{\rm m}_\eta}^2 + {m^{\rm m}_{\eta'}}^2 \right) = \left(m^2_\eta + m^2_{\eta'} \right) + \frac{N_c g^4}{192\pi^2} \left(3x^2 X + 6y^2 Y \right) \ ; \ X = 1 + 4\log\left(\frac{g\sigma_x}{2M}\right) \ , \ Y = 1 + 4\log\left(\frac{g\sigma_y}{\sqrt{2}M}\right)
\end{aligned} \tag{23}$$

λ_2 and c are obtained as

$$\lambda_2 = \frac{3\left(2f_K - f_\pi\right) {m^{\rm m}_K}^2 - \left(2f_K + f_\pi\right) {m^{\rm m}_\pi}^2 - 2\left({m^{\rm m}_\eta}^2 + {m^{\rm m}_{\eta'}}^2 \right)\left(f_K - f_\pi\right)}{\left(3f_\pi^2 + 8 f_K \left(f_K - f_\pi\right)\right)\left(f_K - f_\pi\right)} \ ; \ c = \frac{{m^{\rm m}_K}^2 - {m^{\rm m}_\pi}^2}{f_K - f_\pi} - \lambda_2 \left(2f_K - f_\pi\right) \tag{24}$$

Putting the value of ${m^{\rm m}_\pi}^2$, ${m^{\rm m}_K}^2$ and $\left({m^{\rm m}_\eta}^2 + {m^{\rm m}_{\eta'}}^2 \right)$ in Eq.(24) we find

$$\begin{aligned}
\lambda_2 &= \lambda_{2s} + \lambda_{2+} + n\left(1 + 4\log\left(\frac{g\left(2f_K - f_\pi\right)}{2M}\right)\right) \ where \ \lambda_{2+} = \frac{n {f_\pi}^2}{f_K\left(f_K - f_\pi\right)} \log\left(\frac{2\ f_K - f_\pi}{f_\pi}\right), n = \frac{N_c g^4}{32\pi^2}; \\
\lambda_{2s} &= \frac{3\left(2f_K - f_\pi\right) m^2_K - \left(2f_K + f_\pi\right) m^2_\pi - 2\left(m^2_\eta + m^2_{\eta'}\right)\left(f_K - f_\pi\right)}{\left(3f_\pi^2 + 8 f_K \left(f_K - f_\pi\right)\right)\left(f_K - f_\pi\right)} \ and \ c = \frac{{m_K}^2 - {m_\pi}^2}{f_K - f_\pi} - \lambda_{2s}\left(2f_K - f_\pi\right)
\end{aligned} \tag{25}$$

The fermionic vacuum modifications ${\delta m^{\rm v}_{\alpha,ab}}^2$ of the meson masses have a logarithmic dependence on the renormalization scale M. We denote the parameter λ_2 determined in the earlier QM and PQM model calculations in Ref. [28, 58, 59] by λ_{2s}. The proper renormalization of fermionic vacuum leads to an addition of a constant (λ_{2+}+n) contribution to the λ_{2s}. Apart from it, the λ_2 in Eq.(25) has a renormalization scale M dependent contribution in the present evaluation. Substituting this value of λ_2 in U(σ_x, σ_y), we find that the logarithmic M dependence of λ_2 completely cancels the scale dependence of $\Omega^{\rm vac}_{q\bar{q}}$ term in Eq.(20) and the chiral part of the total effective potential becomes free of any renormalization scale dependence. We get the complete

cancellation of M dependence in the evaluation of c also and finally its value turns out to be the same as in the QM model. Further when this value of λ_2 is substituted in the expressions of meson masses (as given in Table II of Ref.[28]) obtained from the second derivative of the pure mesonic potential $\mathrm{U}(\sigma_x, \sigma_y)$, the logarithmic M dependence of λ_2 neatly cancels with the scale dependence already existing in the mass modifications ${\delta m^{\mathrm{v}}_{\alpha,ab}}^2$ due to the fermionic vacuum correction and the final expression of meson masses $m^2_{\alpha,ab}$ becomes free of any scale dependence when these two contributions are added together. The expressions of the scale independent scalar and pseduscalar meson masses that we will be using in the present calculation are given in Table II. $\lambda_{2s} + \lambda_{2+}$ has been denoted by λ_{v}.

The chiral part of the PQM/PQMVT model has six input parameters and therefore require six known quantities as input. In general m_π, m_K, the pion and kaon decay constant f_π, f_K, mass square of η, η' and m_σ are used to fix these parameters. The parameters are fitted such that in vacuum, the model produces observed pion mass 138 MeV, kaon mass 496 MeV and $m'_\eta = 963(138)$ MeV, $m_\eta = 539(634.8)$ MeV for the case with the presence (absence c=0) of axial anomaly term c. We have already obtained the λ_{2s} and c, numerical values of λ_{2+} and n are obtained using $f_\pi = 92.4, f_K = 113$ MeV and $N_c = 3$. Using the expression of m^2_π, we express m^2 in terms of λ_1. With $m_\sigma = 600$ MeV, the expression of m^2_σ given in Table II is exploited to yield the numerical value of λ_1. In the present work, the λ_{2s} and c are the same as in [59], the value of h_x and h_y are also not affected by the fermionic vacuum correction. The parameters which are modified by the fermionic vacuum correction are m^2, λ_1 and λ_2. Table II A summarizes the parameters in different model scenarios.

We finally obtain the following scale independent chiral part of the effective potential as:

$$\Omega(\sigma_x,\sigma_y) = \frac{m^2}{2}\left(\sigma_x^2+\sigma_y^2\right) - h_x\sigma_x - h_y\sigma_y - \frac{c}{2\sqrt{2}}\sigma_x^2\sigma_y + \frac{\lambda_1}{2}\sigma_x^2\sigma_y^2 + \frac{\lambda_1}{4}\left(\sigma_x^4+\sigma_y^4\right) + \frac{(\lambda_{2\mathrm{v}}+n)}{8}\left(\sigma_x^4+2\sigma_y^4\right) - \frac{n\sigma_x^4}{2}\log\left(\frac{\sigma_x^4}{(2f_K-f_\pi)}\right) - n\sigma_y^4\log\left(\frac{\sqrt{2}\,\sigma_y^4}{(2f_K-f_\pi)}\right) \quad (26)$$

Now the thermodynamic grand potential in the presence of appropriately renormalized fermionic vacuum contribution in the PQMVT model will be written as

$$\Omega_{\mathrm{MF}}(T,\mu;\sigma_x,\sigma_y,\Phi,\Phi^*) = \mathcal{U}(T;\Phi,\Phi^*) + \Omega(\sigma_x,\sigma_y) + \Omega^{\mathrm{T}}_{q\bar{q}}(T,\mu;\sigma_x,\sigma_y,\Phi,\Phi^*) \quad (27)$$

One can get the quark condensates σ_x, σ_y and Polyakov loop expectation values Φ, Φ^* by searching the global minima of the grand potential for a given value of temperature T and chemical potential μ.

$$\frac{\partial\Omega}{\partial\sigma_x} = \frac{\partial\Omega}{\partial\sigma_y} = \frac{\partial\Omega}{\partial\Phi} = \frac{\partial\Omega}{\partial\Phi^*}\bigg|_{\sigma_x=\bar{\sigma}_x,\sigma_y=\bar{\sigma}_y,\Phi=\bar{\Phi},\Phi^*=\bar{\Phi}^*} = 0\ . \quad (28)$$

The diagonalization of (0 - 8) component of mass matrix gives masses of σ and f_0 mesons in scalar sector and masses of η' and η in pseudoscalar sector. The scalar mixing angle θ_s and pseudoscalar mixing angle θ_p are given by,

$$\tan 2\theta_\alpha = \left(\frac{2m^2_{\alpha,08}}{m^2_{\alpha,00}-m^2_{\alpha,88}}\right) \quad (29)$$

The meson masses are further modified in medium at finite temperature by the quark contributions in the grand potential. In order to calculate the second derivative Eq.(21) for evaluating the finite temperature quark contribution in the presence of Polyakov loop potential, the complete dependence of all scalar and pseudoscalar meson fields in Eq.(6) has to be taken into account. We have to diagonalize the resulting quark mass matrix. The expression for the meson mass modification due to the quark contribution at finite temperature in the QM and PQM model, has already been evaluated respectively in Ref. [59] and [28] In the following, we give the expression of mass modification due to the quark contribution at finite temperature in the PQM model as:

$$\delta m^2_{\alpha,ab} = \frac{\partial^2\Omega_{\bar{q}q}(T,\mu)}{\partial\xi_{\alpha,a}\partial\xi_{\alpha,b}}\Big|_{min} = 3\sum_{f=x,y}\int\frac{d^3p}{(2\pi)^3}\frac{1}{E_f}\left[(A^+_f+A^-_f)\left(m^2_{f,ab}-\frac{m^2_{f,a}m^2_{f,b}}{2E_f^2}\right) + (B^+_f+B^-_f)\left(\frac{m^2_{f,a}m^2_{f,b}}{2E_fT}\right)\right] \quad (30)$$

The notations $A^\pm_f$ and $B^\pm_f$ have the following definitions

$$A^+_f = \frac{\Phi e^{-E^+_f/T} + 2\Phi^* e^{-2E^+_f/T} + e^{-3E^+_f/T}}{g^+_f} \quad (31)$$

$$A^-_f = \frac{\Phi^* e^{-E^-_f/T} + 2\Phi e^{-2E^-_f/T} + e^{-3E^-_f/T}}{g^-_f} \quad (32)$$

and $B^\pm_f = 3(A^\pm_f)^2 - C^\pm_f$, where we again define

$$C^+_f = \frac{\Phi e^{-E^+_f/T} + 4\Phi^* e^{-2E^+_f/T} + 3e^{-3E^+_f/T}}{g^+_f} \quad (33)$$

$$C^-_f = \frac{\Phi^* e^{-E^-_f/T} + 4\Phi e^{-2E^-_f/T} + 3e^{-3E^-_f/T}}{g^-_f} \quad (34)$$

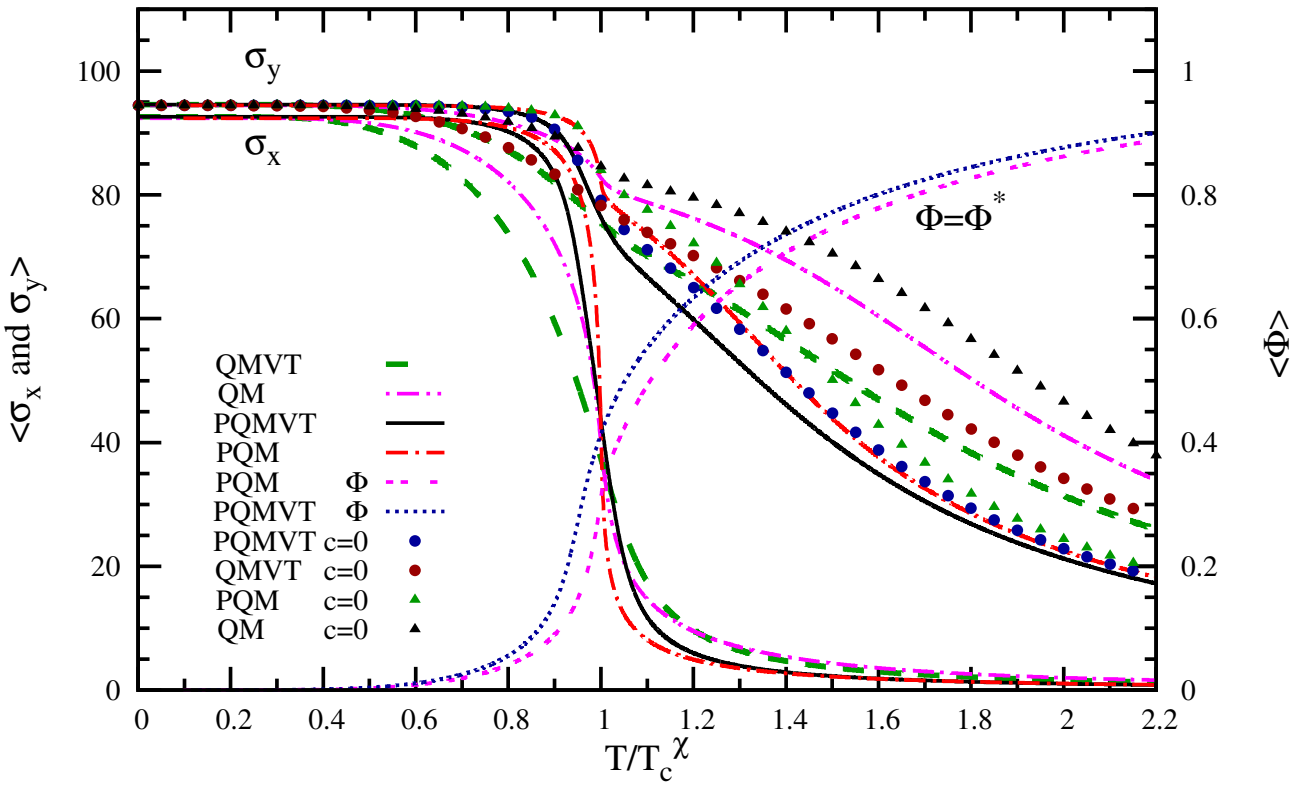

FIG. 1: The variations of nonstrange σ_x, strange σ_y condensates with respect to the relative temperature scale (T/T_c^{χ}) at zero chemical potential ($\mu = 0$) in the QM,QMVT ,PQM and PQMVT models have been shown. The magenta lines with dash double dots , dark green lines with thick long dash and red lines with dash dot, represent the respective variations in QM, QMVT and PQM models while the solid black lines represent the PQMVT model variations. Four such lines in the upper half of the figure represent the strange σ_y condensates while the same line types in the lower half represent the nonstrange σ_x condensates for computations done with the axial anomaly (non-zero c). In the upper half of the figure, the first lower line with dark blue solid circular dots and then the second lower line with dark green solid triangular dots show the respective variations of the σ_y in the PQMVT and PQM models while the upper line with dark red solid circular dots and the uppermost line with black solid triangular dots represent the respective σ_y variations in the QMVT and QM models when axial anomaly term is absent i.e. $c = 0$. The expectation value of the Polyakov loop $\langle\Phi\rangle$, is shown in the right hand side plots, dark blue small dash line represents the Φ variation in the PQMVT model while the double dash magenta line represents the Φ variation in the PQM model.

	QM	QMVT	PQM	PQMVT
T_c^{χ}(MeV)	146.1	171.1	205.8	216.5
T_s^{χ}(MeV)	$248.3 \pm .5$	247.8 ± 1.0	274 ± 1.5	$269. \pm 1.5$
T_c^{Φ} (MeV)	–	–	205.6	205.6

TABLE IV: The characteristic temperature (pseudo critical temperature) for the chiral transition in the nonstrange sector T_c^{χ}, strange sector T_s^{χ} and confinement-deconfinement transition T_c^{Φ}, in QM, QMVT, PQM and PQMVT model.

V. FERMIONIC VACUUM CORRECTION AND CHIRAL RESTORATION

We are investigating the effect of fermionic vacuum fluctuation on the restoration of chiral symmetry when it is properly accounted for in the $2 + 1$ flavor quark meson model and PQM model at finite temperature and zero chemical potential with and without axial $U_A(1)$ breaking. We have compared the results of present computations in the QMVT and PQMVT models with the already existing calculations in the quark meson model and PQM model [28, 59]. The interplay of the effect of $U_A(1)$ axial restoration and chiral symmetry restoration in the influence of fermionic vacuum fluctuation has been demonstrated and compared with in different model scenarios through the temperature variation of strange, nonstrange chiral condensates, meson masses and mixing angles. The $U_A(1)$ axial breaking term is constant throughout the computation. The value of Yukawa coupling g has been fixed from the nonstrange constituent quark mass $m_q =$ 300 MeV and is equal to 6.5. This predicts the strange quark mass $m_s \backsimeq 433$ MeV.

A. Condensates and fermionic vacuum correction

The solutions of the gap equations (Eq.28) yield the temperature dependence of the Polyakov loop expectation value $\langle\Phi\rangle$, nonstrange and strange condensates at zero chemical potential and the inflection points of these order parameters respectively give the characteristic temperature (pseudocritical - temperature) for the confinement - deconfinement transition T_c^{Φ}, the chiral transition in the nonstrange T_c^{χ} and strange sector T_s^{χ}. Numerical values of pseudo critical temperatures for different transitions in quark meson (QM), QMVT, PQM and PQMVT models, are given in Table V. It is evident from the Table V that the chiral crossover transition at $\mu = 0$ shifts to higher temperatures T_c^{χ} due to the fermionic vacuum correction. Since the thermal fermionic contributions to the effective potential are suppressed due to the presence of the Polyakov loop, the chiral transition gets delayed and as we already know, the $\mu = 0$ crossover occurs at a significantly higher temperature [28, 63] in PQM model. The incorporation of fermionic vacuum fluctuation in the effective potential of QM model also changes the model parameters such that the chiral transition gets delayed and the QMVT model T_c^{χ} increases by 25 MeV over its QM model value, only due to the effect of the fermionic vacuum correction. Further its influence, gives highest value of T_c^{χ} in PQMVT model. Here it is relevant to recall that larger values of m_σ and T_0 also shift the chiral and deconfinement transition temperatures to higher values. We take m_σ and T_0 as 600.0 and 270.0 MeV respectively in the present calculation in order to compare results with our earlier work in the QM and PQM models in Ref. [28]. Further with these parameter sets, using different versions of Polyakov loop potential in PQM model, one gets coincident chiral and deconfinement crossover transitions [63]. We notice that the fermionic vacuum correction does not affect the confinement-deconfinement crossover transition temperature and T_c^{Φ} has the same value of 205.6 MeV in both the models PQM as well as PQMVT. But the chiral crossover transition in the non-strange sector does not remain coincident with the deconfinement transition due to the fermionic vacuum fluctuation and registering an increase of 11 MeV over the deconfinement crossover temperature T_c^{Φ}=205.6 MeV, the PQMVT model T_c^{χ} becomes 216.5 MeV, as shown in Table V.

We compare the QMVT(PQMVT) model calculations with the corresponding results in the QM(PQM) model on a relative temperature scale T/T_c^{χ}. This is justified because absolute comparison of the characteristic temperatures between two models of the same universality class can not be made according to Ginsburg-Landau effective theory [53]. Since our investigation is focused on identifying the effective symmetry restoration trends due to the influence of fermionic vacuum fluctuations, we will be comparing the mesonic observables below and above T_c^{χ}.

The condensates start with the values $\sigma_x = 92.4$ MeV and σ_y =94.5 MeV at $T = 0$ in Fig.1 . The influence of $U_A(1)$ anomaly (with zero or non-zero value of c) on the behavior of the nonstrange condensate is negligible. The σ_x variation which is sharpest in the $T/T_c^{\chi} = 0.8$ to 1.4 range in the PQM model (dash dot line in red), becomes smoother in the PQMVT model (solid black line) due to the effect of fermionic vacuum term. In the absence of Polyakov loop, the QM model (dash double dot line in magenta) σ_x temperature variation becomes quite smooth in the QMVT model (thick long dash line in dark green), only because of the fermionic vacuum correction. The variation of strange condensate σ_y in PQM model (dash dot line in red) shows an early and significant melting due to the influence of Polyakov loop potential when calculations are done with axial anomaly [28]. It is evident from the upper half black solid line in Fig.1 that the corresponding melting of σ_y is enhanced due to the fermionic vacuum correction and we obtain the largest degree of strange condensate melting in PQMVT model. In the influence of fermionic vacuum correction only, the modification in the melting of strange condensate σ_y is quite larger when we compare the upper half thick long dash line (dark green) in QMVT model with the dash double dot line (magenta) obtained in QM model. When we compare the respective temperature variations of σ_y represented by the filled circular dots line in dark blue (red) color for the PQMVT (QMVT) model with the filled triangular dots line in dark green (black) color for the PQM (QM) model, we conclude that the melting of the strange condensate gets a little reduced in the same proportion in the absence of axial anomaly term i.e. for the $c = 0$ case in all the models PQMVT and PQM, QMVT and QM.

Curves starting from the right end of the plot represent the temperature variation of the Polyakov loop expectation value $\langle\Phi\rangle$. Line with small double dash (magenta) denote the Φ variation in PQM model while line with small dash (dark blue) depict the PQMVT model Φ variation. Here we recall that the improved ansatz of the logarithmic polyakov loop potential [8, 34, 35, 43] avoids the Φ expectation value higher than one and hence describes the dynamics of gluons more effectively.

The chiral crossover transition in the strange sector is lot more smooth and weak in comparison to the corresponding chiral transition in non-strange sector in all the models due to the large constituent mass of the strange quark $m_s = 433$ MeV. The variation of the temperature derivative of σ_y shows two peaks in all the models, the first peak is higher and sharper because it is driven by the chiral crossover transition dynamics in the non strange sector. The crossover temperature T_s^{χ} in the strange sector is identified by locating the position of the second peak which is quite broad, smooth and flat over a small temperature range in all the models. Though we have not shown the temperature variation of the temperature derivative of σ_y in this work, we

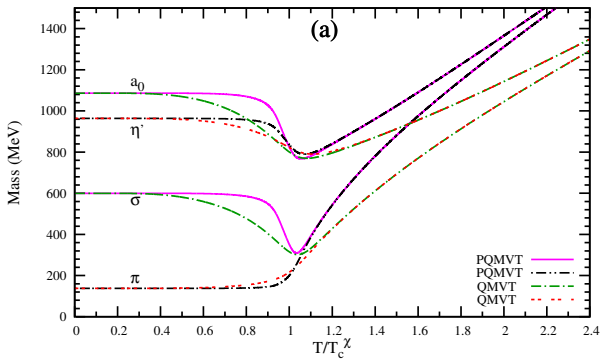

(a)With $U_A(1)$ anomaly term

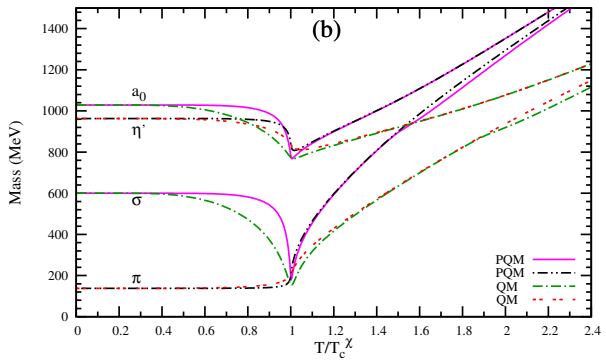

(b)With $U_A(1)$ anomaly term

FIG. 2: Mass variations for the chiral partners (σ, π) and (a_0, η') on the reduced temperature (T/T_c^χ) scale at $\mu = 0$, are plotted in Fig.2(a) for the PQMVT and QMVT model and the corresponding mass variations in the PQM and QM model, are plotted in Fig.2(b). The axial anomaly coefficient c has a constant non-zero value in these computations. The σ and a_0 mass variations are depicted by solid line magenta color plots and dark green line with dash dot plots respectively in the PQMVT (PQM) model and the QMVT (QM) model in the left panel (right panel) while the π and η' mass variations are denoted by the dash double dot black line plots and double dash red line plots respectively in the PQMVT (PQM) model and the QMVT (QM) model in the left panel (right panel).

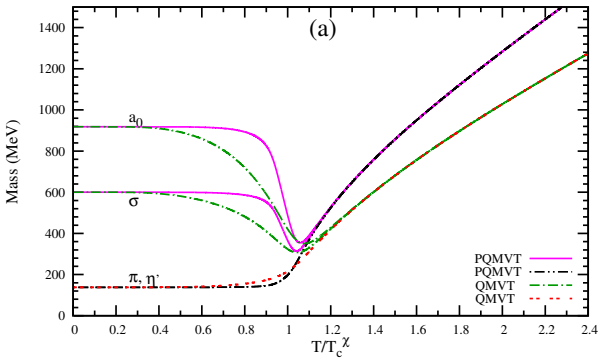

(a)Without $U_A(1)$ anomaly term

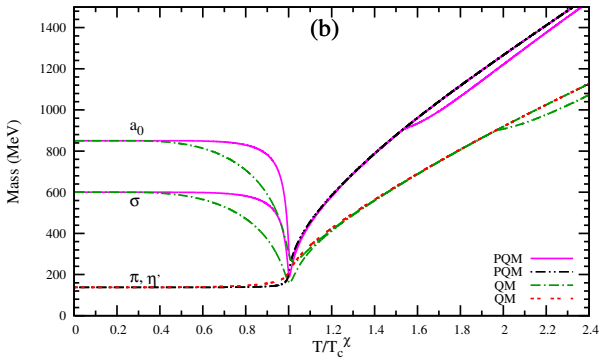

(b)Without $U_A(1)$ anomaly term

FIG. 3: The line types in Fig.3(a) and in Fig.3(b) represent the same mass variations as depicted in Fig.2 but here in these computations the axial anomaly term is absent i.e. $c = 0$.

show the ambiguity in the identification of second peak by indicating the flatness range for T_s^χ in Table V. As discussed above, the earliest and largest but smoother melting of strange condensate is obtained in the PQMVT model with T_s^χ= 269.0 ± 1.5 MeV. It will have an interesting physical consequence in the early setting up of a smoother mass degeneration trend in masses of the chiral partners (K, κ) and (η, f_0) and in the early emergence of a smoother $U_A(1)$ restoration trend.

B. Meson Mass Variations

The expressions of the vacuum masses in the QMVT model evaluated after including the contributions from the fermionic vacuum fluctuation for the scalar and pseudoscalar mesons, are given in Table II. The corresponding vacuum meson mass expressions for the pure QM model (with no fermionic vacuum correction) are already given in Table II of Ref. [28]. When the finite temperature mass modifications due to the quark-antiquark contribution in the QM model (evaluated in [59]), are added to the vacuum mass expressions in the QMVT and QM model, we get the total value of the finite temperature meson masses in the respective models. Similarly when the finite temperature mass modifications due to the $q\bar{q}$ contribution calculated in the presence of Polyakov loop potential in Eq.(30), are added to the vacuum masses as obtained in the QMVT and QM model, we get the final value of the meson masses in the PQMVT and PQM model. In the presence of axial $U_A(1)$ anomaly, the respective mass variations in the PQMVT as well as QMVT model and the PQM as well as QM model for the chiral partners (σ,π) and

(a_0,η'), are plotted in Fig.2(a) and Fig.2(b) respectively and the corresponding mass variations for the chiral partners (η,f_0) and (K,κ) are plotted respectively in Fig.4(a) and Fig.4(b). In the absence of the $U_A(1)$ axial anomaly (i.e.for c=0), the corresponding model plots for the chiral partners (σ,π) and (a_0,η') are given in Fig.3(a) and Fig.3(b) respectively while Fig.5(a) and Fig.5(b) give the respective plots in the same model sets for the chiral partners (η,f_0) and (K,κ). In the influence of fermionic vacuum correction, the sharpest mass degeneration in PQM model computations in Fig.2(b) for (σ,π) and (a_0,η') mesons, becomes quite smooth in the PQMVT model in Fig.2(a) and here the most smooth mass degeneration can be seen in the QMVT model due to the absence of Polyakov loop potential. We conclude from the behavior of these chiral partners that the net effect of the fermionic vacuum correction in the PQM and QM model, is to make a smoother but more effective occurrence of chiral $SU_L(2)\times SU_R(2)$ symmetry restoration. Further in comparison to PQM and QM models, the degenerate σ and π meson masses in the PQMVT and QMVT models, show closer convergence towards the degenerate masses of a_0 and η' for higher $T/T_c^\chi > 1$.

We notice the similar trend of smoother but more effective mass degeneration for the chiral partners (η,f_0) and (K, κ) in Fig.4(a) due to the fermionic vacuum effect. In the PQM (QM) model, the f_0 mass intersects the η mass nearly at $T/T_c^\chi = 1.4(1.8)$ and becomes smaller than the m_η developing a kink like structure after crossing it for higher values of the reduced temperature $T/T_c^\chi > 1.4(1.8)$ in Fig.4(b). Further the f_0 meson becomes degenerate with (K, κ) and η again at $T/T_c^\chi > 1.8(2.3)$. It is important to emphasize that this kink-like mass crossing behavior of f_0 meson altogether disappears from the PQMVT (QMVT) model mass variations of f_0 and η mesons in Fig.4(a) due to the noteworthy effect of the fermionic vacuum correction. Here the f_0 meson becomes degenerate with the (K, κ) and η mesons earlier at $T/T_c^\chi > 1.6(1.9)$ and remains so forever. This trend of mass degeneration reflects the effect of fermionic vacuum fluctuation on the chiral symmetry restoration in the strange sector and it results due to the smoother but larger (largest in the PQMVT model) melting of the strange condensate in Fig.1. Here it is worthwhile to recall that the breaking of $U_A(1)$ axial symmetry, generates the mass gap between the two sets of the chiral partners, (σ, π) and (a_0, η') i.e. $m_\pi = m_\sigma < m_{a_0} = m_{\eta'}$ for $T/T_C^\chi > 1$. This results due to the opposite sign of the anomaly term ($\sqrt{2}c\sigma_y$) in the scalar and pseudoscalar meson masses. Hence the mass gap reduction will be larger due to the larger melting of σ_y for higher $T/T_c^\chi > 1$ and the mass of the degenerated σ, π mesons will converge more closely to the higher mass of the already degenerated a_0, η' mesons. We have already seen this behavior in Fig.2(a). Thus the inclusion of fermionic vacuum fluctuation in the PQM (QM) model also effects an early and smoother set up of the $U_A(1)$ restoration trend.

Here we will be discussing the variations in the masses of the chiral partners when the $U_A(1)$ axial anomaly is absent (c=0). Comparing the plots in Fig.3(a) and Fig.5(a) respectively with those in Fig.3(b) and Fig.5(b), we again find, the same smoother but more effective mass convergence trend for the mass degeneration that we identify as the effect generated by the inclusion of fermionic vacuum fluctuation in the PQMVT and QMVT model. In the absence of the anomaly, the $m_{\eta'} = m_\pi$ in the vacuum and it stays the same at all temperatures in Fig.3(a) and Fig.3(b). Further the mass gap between the chiral partners (σ, π) and (a_0, η') becomes zero and all the four mesons become degenerate at $T/T_c^\chi = 1.0$ in all the models . The T/T_c^χ numerical value, where the K, κ and η masses degenerate in different models, is not influenced by the $U_A(1)$ anomaly as expected since the nonstrange condensate does not have any anomaly dependence. Further, in Fig.5(b), the f_0 mass variation in the PQM (QM) model, does not show the crossing behavior similar to the corresponding mass variation computed in the presence of the axial anomaly. Here the f_0 mass does not become completely degenerate with the m_η though it becomes very close (nearly touches) to the η mass variation when $T/T_c^\chi \sim 1.6(2.0)$ and afterwards f_0 takes slightly larger value than m_η. In the PQMVT (QMVT) model in Fig.5(a), the f_0 mass variation becomes completely degenerate with the m_η when $T/T_c^\chi \sim 1.9(2.3)$ and does not show any crossing behavior. Further in the absence of anomaly we also note that the mass of f_0 in vacuum increases by about 60 MeV.

Here we mention another noteworthy finding. In the influence of the fermionic vacuum correction, the scalar particle vacuum mass increases to 1086.26(917.93) MeV for the a_0 meson and decreases to 1143.92(1203.16) MeV for the f_0 meson in the presence(absence) of axial anomaly in the PQMVT and QMVT models from the respective vacuum mass value of m_{a_0}=1028.7(850.5) MeV and m_{f_0}=1221.1(1282.3) MeV in the PQM and QM model. We recall further that the mass variations of scalar σ and f_0 show the kink around $T/T_c^\chi = 1.8$ in the QM model while it is seen around $T/T_c^\chi = 1.4$ in PQM model. The kink generation in the PQM and QM model results because the meson masses interchange their identities for higher values on the reduced temperature scale [28, 59]. It is worth emphasizing that the kink in the scalar σ and f_0 meson masses, gets completely washed out by the presence of fermionic vacuum fluctuation in the PQMVT and QMVT model and we get a completely smooth mass degeneration trend in these models without any crossing or anti-crossing of meson masses. In order to have a proper perspective of the kink behavior in the PQM and QM model mass variations and of the complete washing out of the kinks in PQMVT and QMVT model results, one has to investigate, analyze and compare the scalar and pseudoscalar meson mixing angles.

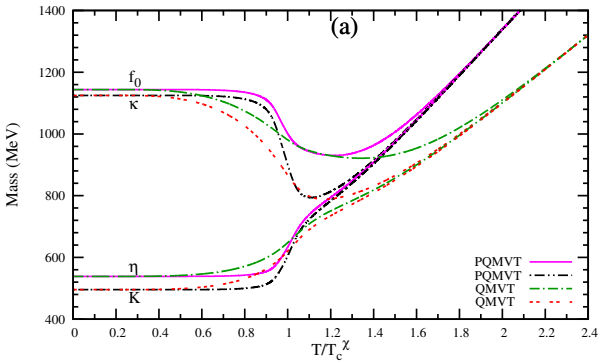

(a)With $U_A(1)$ anomaly term

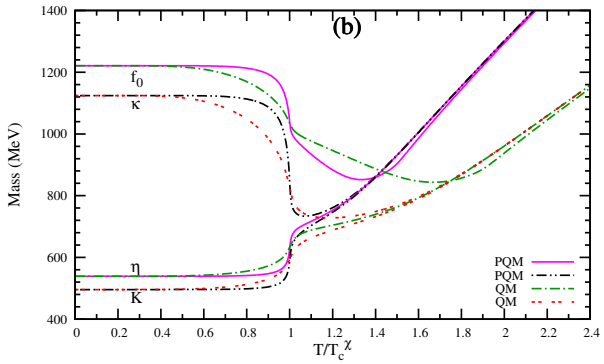

(b)With $U_A(1)$ anomaly term

FIG. 4: Mass variations for the chiral partners (η, f_0) and (K, κ) on the reduced temperature (T/T_c^χ) scale at $\mu = 0$, are plotted in Fig.4(a) for the PQMVT and QMVT model and the corresponding mass variations in the PQM and QM model, are plotted in Fig.4(b). The axial anomaly coefficient c has a constant non-zero value in these computations. The η and f_0 mass variations are depicted by the solid line in magenta color plots and dash dot line dark green color plots respectively in the PQMVT (PQM) model and the QMVT (QM) model in the left panel (right panel) while the K and κ mass variations are denoted by the dash double dot black line plots and double dash red line plots respectively in the PQMVT (PQM) model and the QMVT (QM) model in the left panel (right panel)

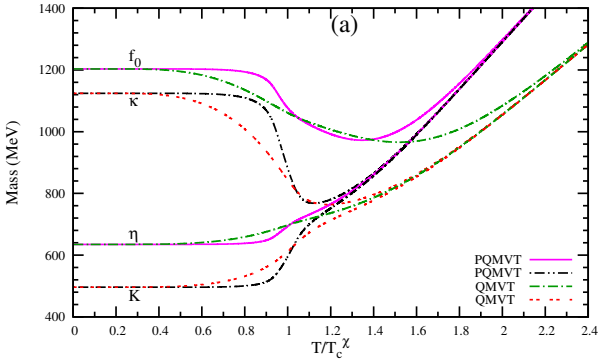

(a)Without $U_A(1)$ anomaly term

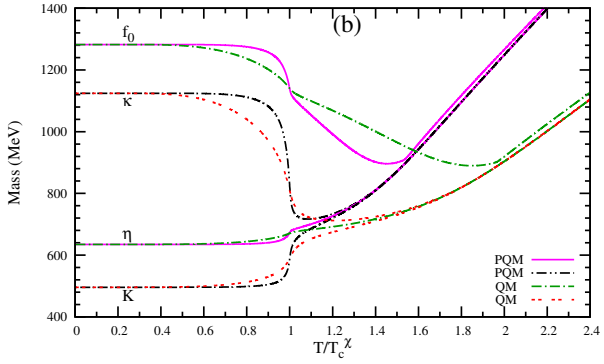

(b)Without $U_A(1)$ anomaly term

FIG. 5: The line types in Fig.5(a) and in Fig.5(b) represent the same mass variations as depicted in Fig.4 but here in these computations the axial anomaly term is absent i.e. $c = 0$.

C. Meson Mixing Angle Variations

We will finally be investigating the behavior of the scalar θ_S and pseudoscalar θ_P mixing angles on the relative temperature scale. In the presence of axial anomaly, the lower(upper) solid lines in magenta color and dash dot black lines depict the $\theta_P(\theta_S)$ variations respectively in the PQMVT(PQM) and QMVT(QM) model computations in the Fig.6(a) (Fig.6(b)). In the absence of axial anomaly, the dash double dot line in dark green color and double dash line in red color represent the scalar θ_S mixing angle variations respectively in the PQMVT(PQM) and QMVT(QM) model computations in the Fig.6(a) (Fig.6(b)). The pseudoscalar θ_P mixing angle variations for this case are constant and are shown by black dash line and filled circular dots in blue color respectively in the PQMVT(PQM) and QMVT(QM) model calculations in the Fig.6(a) (Fig.6(b)). Comparing the PQMVT and QMVT model variations of θ_P and θ_S in Fig.6(a) with the corresponding PQM and QM model results shown in Fig.6(b), we infer that the fermionic vacuum correction significantly modifies the axial $U_A(1)$ restoration pattern.

The nonstrange and strange quark mixing is strong, and at $T = 0$ one gets the pseudoscalar mixing angle $\theta_P = -5^\circ$ in all the models which remains almost constant in the chiral broken phase. The θ_P variation near $T/T_c^\chi = 1$ in the PQMVT model in Fig.6(a) develops a small dip and then smoothly starts the approach toward the ideal mixing angle $\theta_P \rightarrow \arctan\frac{1}{\sqrt{2}} \sim 35^\circ$, the corresponding $\Phi_P = 90^\circ$. Here Φ_P is the pseudoscalar mixing angle in the

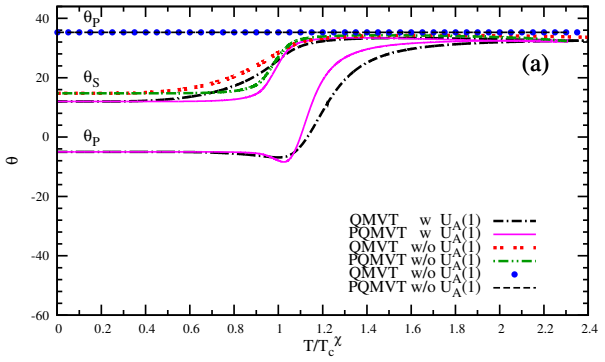

(a)Scalar and Psedoscalar mixing angle variations in PQMVT and QMVT model

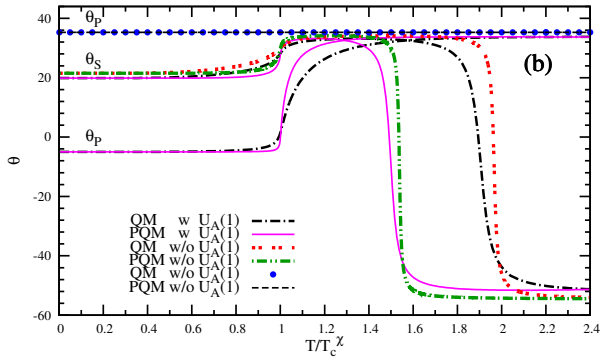

(b)Scalar and Psedoscalar mixing angle variations in PQM and QM model

FIG. 6: In the presence of axial anomaly, the lower(upper) magenta color solid lines and dash dot black lines depict the $\theta_P(\theta_S)$ variations respectively in the PQMVT and QMVT model computations in the Fig.6(a) while the same line types represent the corresponding variations respectively for the PQM and QM model in (Fig.6(b)). In the absence of axial anomaly, the dash double dot line in dark green color and double dash line in red color represent the scalar θ_S mixing angle variations respectively in the PQMVT and QMVT model computations in the Fig.6(a) while the same line types represent the corresponding variations respectively for the PQM and QM model in (Fig.6(b)). The pseudoscalar θ_P mixing angle variations for this case are constant and are shown by black dash line and filled circular dots in blue color respectively in the PQMVT and QMVT model calculations in the Fig.6(a) while the same line types represent the corresponding variations respectively for the PQM and QM model in Fig.6(b).

strange nonstrange basis (see Ref.[59] for details). In computations with the presence of axial anomaly for $T/T_c^\chi > 1$, the pseudoscalar mixing angle approaches its ideal value more smoothly in the PQMVT and QMVT model when compared with the corresponding result in the PQM and QM model in Fig.6(b). This approach is sharpest in the PQM model.

The η and η' mesons become a purely strange η_S and nonstrange η_{NS} quark system as a consequence of the ideal pseudoscalar mixing which gets fully achieved at higher values of the reduced temperature. In order to show this and make comparisons, the mass variations for the physical η, η' and the nonstrange-strange η_{NS}, η_S complex, are plotted for the PQMVT and QMVT model in Fig.7(a) and the plots for the PQM and QM model are shown in Fig.7(b). Mass formula $m_{\eta_{NS}}$ and m_{η_S} are given in Table II. In the $m_{\eta'}$ approach to $m_{\eta_{NS}}$ and the m_η approach to m_{η_S} around $T/T_c^\chi = 1$, the most smooth and smoother mass convergence trend is seen respectively in the QMVT and PQMVT model in Fig.7(a) because of the influence of fermionic vacuum fluctuation. This mass convergence trend is sharp most in the PQM model in Fig.7(b) due to the influence of Polyakov loop potential. The smallest mass difference between the $m_{\eta'}$ (which is degenerate with $m_{\eta_{NS}}$) and m_η (which is degenerate with m_{η_S}) for $T/T_c^\chi > 1$ results in the PQMVT model. It means that we are getting the most effective $U_A(1)$ restoration trend in the PQMVT model for the pseudoscalar sector.

Due to the effect of fermionic vacuum correction, the scalar mixing angle θ_S value in vacuum (i.e. at $T = 0$) decreases to 11.98(14.75) degree in the presence(absence) of axial anomaly in the PQMVT and QMVT models in Fig.6(a) from its value of 19.86(21.5) degree in Fig.6(b) for PQM and QM models. Growth of θ_S to its ideal value starts near $T/T_c^\chi = 1$ in all the models but this growth is smoother in PQMVT and QMVT model. In the chirally symmetric phase of the PQMVT and QMVT model in Fig.6(a), the scalar mixing angle θ_S smoothly approaches the ideal value of ($\theta_S \sim 35^\circ$) mixing angel for higher temperatures for both the cases with and without the axial anomaly. We thus conclude that the behavior of θ_S, gets completely modified by the presence of fermionic vacuum correction in the PQMVT and QMVT model and instead of dropping down to negative values (as in the PQM and QM model) in the chiral symmetry restored phase, θ_S approaches the ideal mixing angle value smoothly similar to the temperature variation of the pseudoscalar θ_P mixing angle for computations with the axial anomaly.

In the chirally symmetric phase of the PQM and QM model in Fig.6(b), the scalar mixing angle drops down to $\theta_S \sim -51^\circ(-54^\circ)$ for higher temperatures in the presence (absence) of $U_A(1)$ axial symmetry breaking term. This drop happens around $T/T_c^\chi \sim 1.5(1.9)$ in the PQM(QM) model for non zero c and similar drop for the calculations without axial anomaly occurs at a little higher value of T/T_c^χ. It is already reported and discussed in Ref.[28, 59] that this behavior results because the masses of the physical σ and f_0 anti cross and the nonstrange - strange ($\sigma_{NS} - \sigma_S$) system masses cross in the close vicinity of the above mentioned reduced temperatures. After anti crossing the physical σ becomes identical with pure strange quark system σ_S while the physical f_0 becomes

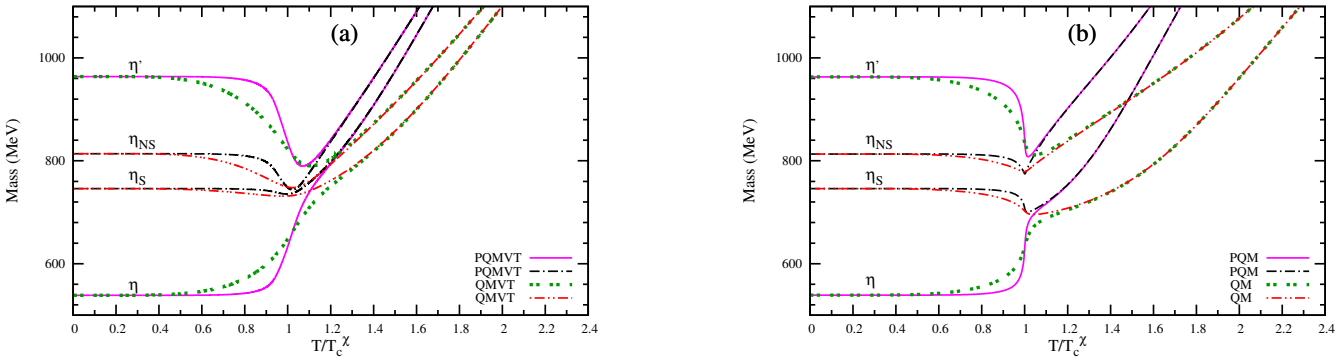

(a)With $U_A(1)$ anomaly term (b)With $U_A(1)$ anomaly term

FIG. 7: Shows the mass variations for the physical η', η and the nonstrange-strange η_{NS}, η_S complex, on the reduced temperature scale (T/T_c^{χ}) at zero chemical potential $(\mu = 0)$. Fig.8(a) shows the results for PQMVT and QMVT model and line types for mass variations are labeled. Fig.8(b) shows the mass variations for the PQM and QM model with labeled line types.

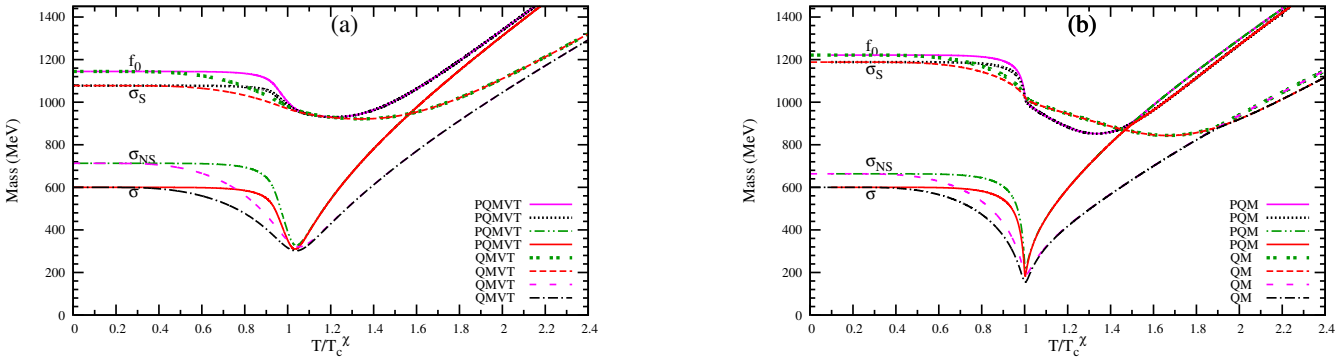

(a)With $U_A(1)$ anomaly term (b)With $U_A(1)$ anomaly term

FIG. 8: Shows the mass variations for the physical σ, f_0 and the nonstrange-strange σ_{NS}, σ_S complex, on the reduced temperature scale (T/T_c^{χ}) at zero chemical potential $(\mu = 0)$. Fig.8(a) shows the results for PQMVT and QMVT model and line types for mass variations are labeled. Fig.8(b) shows the mass variations for the PQM and QM model with labeled line types. Here, the masses of the physical σ and f_0 anti cross and the nonstrange-strange $\sigma_{NS} - \sigma_S$ system masses cross.

degenerate with the pure nonstrange quark system σ_{NS}. In order to show this crossing-anticrossing behavior in the presence of axial anomaly, we have plotted in Fig.8(b), the PQM and QM model mass variations for the physical σ and f_0 and the nonstrange-strange σ_{NS}, σ_S complex. Since the effect of fermionic vacuum fluctuation drastically modifies the θ_S behavior for higher temperatures, the masses of the physical σ and f_0 do not anti cross and the nonstrange - strange $(\sigma_{NS} - \sigma_S)$ system masses do not cross for higher values on the reduced temperature scale and the σ becomes identical with the pure nonstrange quark system σ_{NS} while the physical f_0 becomes degenerate with the pure strange quark system σ_S, in the PQMVT and QMVT model plots in Fig.8(a)

VI. SUMMARY AND CONCLUSION

In the present work, we have investigated how the inclusion of properly renormalized fermionic vacuum fluctuation in the 2+1 flavor QM and PQM models, modifies the finite temperature behavior of masses and mixing angles of scalar and pseudoscalar mesons. It has been explicitly shown that expressions for the model parameters, meson masses and mixing angles, do not depend on any arbitrary renormalization scale. We explored the qualitative and quantitative effects of fermionic vacuum correction, on the emerging mass degeneration patterns in the temperature variations of masses of the chiral partners in pseudoscalar (π, η, η', K) and scalar (σ, a_0, f_0,κ) meson nonets. From the mass convergence patterns, we identified chiral symmetry and $U_A(1)$ restoration trends and compared them in different

model scenarios.

The temperature variation of the nonstrange, strange condensates and Polyakov loop field Φ at $\mu = 0$ has been obtained from the gap equation in all the models QM, QMVT and PQM, PQMVT. Comparisons indicate that the temperature T_c^χ of the chiral crossover transition in the nonstrange sector shifts to the higher values in the influence of fermionic vacuum correction. The T_c^χ in the QMVT model increases by 25 MeV over its QM model value. We know that the Polyakov loop potential delays the chiral transition and T_c^χ increases significantly in the PQM model. Further one gets coincidence of the deconfinement crossover transition with the chiral crossover transition in the non-strange sector in the PQM model. We find that though the effect of fermionic vacuum fluctuation does not lead to any change in the deconfinement crossover transition temperature (T_c^Φ = 205.6 MeV in both the models; PQM and PQMVT), its influence spoils the above mentioned coincidence of the chiral transition with the deconfinement transition and registering an increase of 11 MeV over the T_c^Φ=205.6 MeV, the T_c^χ in the PQMVT model becomes 216.5 MeV. The σ_x variation which is sharpest in the T/T_c^χ = 0.8 to 1.4 interval in the PQM model becomes smoother in the PQMVT model and in the absence of Polyakov loop, the QM model σ_x temperature variation becomes a lot more smooth in the QMVT model only because of the fermionic vacuum correction. It is already known that the enrichment of QM model with Polyakov loop potential, leads to a larger and significant melting of the strange condensate [28]. The melting of the σ_y is further enhanced due to the presence of fermionic vacuum correction and we obtain the largest but smoother melting of strange condensate in the PQMVT model. The interesting physical consequence of the earlier and larger but smoother melting of the strange condensate will be an early setting up of a smoother mass degeneration trend in the masses of the chiral partners (K, κ) and (η, f_0) and an early emergence of a smoother $U_A(1)$ restoration trend.

The sharpest mass degeneration trend obtained in the PQM model computations for (σ,π) and (a_0,η') mesons, becomes quite smooth in the PQMVT model and the most smooth mass degeneration is seen in the QMVT model due to the absence of Polyakov loop potential. We thus conclude from the behavior of these chiral partners that the net effect of the inclusion of fermionic vacuum correction in the PQM and QM model, is to make a smoother but more effective occurrence of chiral $SU_L(2) \times SU_R(2)$ symmetry restoration transition in the nonstrange sector. Further in comparison to PQM and QM models, the degenerated masses of σ and π mesons in the PQMVT and QMVT models, show closer, smoother and more effective convergence towards the degenerate masses of a_0 and η' for higher $T/T_c^\chi > 1$. This behavior is a consequence of the largest but smoother and earlier melting of the strange condensate in the PQMVT model because the $U_A(1)$ breaking anomaly effect that leads to the mass gap between the two sets of the chiral partners,(σ, π) and (a_0, η') i.e. $m_\pi = m_\sigma < m_{a_0} = m_{\eta'}$ for $T/T_C^\chi > 1$, is proportional to the strange condensate σ_y. Thus the incorporation of fermionic vacuum correction in the PQM and QM models also effects an early set up of $U_A(1)$ restoration trend on the reduced temperature scale.

Similar trend of smoother mass degeneration is noticed in the PQMVT and QMVT model temperature variations of the masses of the chiral partners (η,f_0) and (K, κ). We point out that in the QM and PQM models, the f_0 mass intersects the η mass nearly at T/T_c^χ = 1.4(1.8) and becomes smaller than the m_η developing a kink like structure after crossing it for higher values of the reduced temperature $T/T_c^\chi > 1.4(1.8)$. Further the f_0 meson becomes degenerate with (K, κ) and η again at $T/T_c^\chi > 1.8(2.3)$. It is important to emphasize that this kink-like mass crossing behavior of f_0 meson altogether disappears from the PQMVT (QMVT) model mass variations of f_0 and η mesons due to the noteworthy effect of the fermionic vacuum correction. Here the f_0 meson becomes degenerate with the (K, κ) and η mesons earlier at $T/T_c^\chi > 1.6(1.9)$ and remains so forever. This trend of mass degeneration reflects the effect of fermionic vacuum correction on the chiral symmetry restoration in the strange sector and it results again due to the smooth (smoother) but largest (larger) melting of the strange condensate in the PQMVT(QMVT) model.

For $T/T_c^\chi > 1$ in the presence of axial anomaly, the pseudoscalar mixing angle θ_P approaches its ideal value more smoothly in the PQMVT and QMVT model when compared with the corresponding result in the PQM and QM model. The smallest mass difference between the $m_{\eta'}$ (which is degenerate with $m_{\eta_{NS}}$) and m_η (which is degenerate with m_{η_S}) for $T/T_c\chi > 1$ results in PQMVT model. This again is the evidence of the setting up of the most effective $U_A(1)$ restoration trend in the PQMVT model for the pseudoscalar sector.

Due to the effect of fermionic vacuum correction, the scalar mixing angle θ_S value in vacuum (i.e. at $T = 0$) decreases to 11.98(14.75) degree in the presence(absence) of axial anomaly in the PQMVT and QMVT models from its value of 19.86(21.5) degree for PQM and QM models.

In the chirally symmetric phase of the PQM and QM model, the scalar mixing angle drops down to $\theta_S \sim -51^\circ(-54^\circ)$ for higher temperatures in the presence (absence) of $U_A(1)$ axial anomaly. Due to this drop, the masses of the physical σ and f_0 anti cross and the nonstrange - strange ($\sigma_{NS} - \sigma_S$) system masses cross in the QM and PQM model. The most striking effect of the fermionic vacuum correction is seen in the complete modification of the temperature variation of the scalar mixing angle θ_S in the chirally symmetric phase of the PQMVT and QMVT model. Instead of dropping down to large negative values, it smoothly approaches the ideal value of ($\theta_S \sim 35^\circ$) mixing angel for higher temperatures in the presence as well as absence of axial anomaly. As a consequence, masses of the physical σ and f_0 do not

anti cross and the nonstrange-strange ($\sigma_{NS} - \sigma_S$) system masses do not cross for higher values on the reduced temperature scale in the PQMVT(QMVT) model. σ becomes identical with pure nonstrange quark system σ_{NS} while the physical f_0 becomes degenerate with the pure strange quark system σ_S.

Acknowledgments

Valuable suggestions and computational helps given by Rajarshi Ray during the completion of this work are specially acknowledged. I am very much thankful to Rajarshi Tiwari for helping me in generating good quality colored figures. General physics discussions with Ajit Mohan Srivastava are very helpful. computational support of the computing facility which has been developed by the Nuclear Particle Physics group of the Physics Department, Allahabad University under the Center of Advanced Studies(CAS) funding of UGC, India, is also acknowledged.

[1] L.D.McLerran, B.Svetitsky, Phys. Rev. D**24**, 450 (1981); B.Svetitsky, Phys. Rep. **132**, 1 (1986).
[2] B.Muller, Rep. Prog. Phys. **58**, 611 (1995).
[3] H.Meyer-Ortmanns Rev. Mod. Phys. **68**, 473 (1996).
[4] D. H. Rischke, Prog. Part. Nucl. Phys. **52**, 197 (2004).
[5] A. M. Polyakov, Phys. Lett. **B 72**, 477 (1978).
[6] R. D. Pisarski, Phys. Rev. **D 62** 111501(R) (2000).
[7] B. Layek, A. P. Mishra, A. M. Srivastava and V. K. Tiwari, Phys. Rev. **D 73** 103514 (2006).
[8] O. Kaczmarek, F. Karsch, P. Petreczky and F. Zantow, Phys. Lett. **B 543**, 41 (2002).
[9] F. Karsch, Lect. Notes Phys. **583**, 209 (2002).
[10] Z. Fodor, S. D. Katz, and K. K. Szabo, Phys. Lett. **B 568**, 73 (2003).
[11] C. R. Allton, M. Doring, S. Ejiri, S. J. Hands, O. Kaczmarek, F. Karsch, E Laermann and K. Redlich, Phys. Rev. **D 71**, 054508 (2005).
[12] Y. Aoki, Z. Fodor, S. D. Katz and K. K. Szabo, Phys. Lett. **B 643**, 46 (2006).
[13] F. Karsch, J. Phys. **G 31**, S633 (2005).
[14] F. Karsch, e-Print: arXiv:0701.210 [hep-ph].
[15] M. Cheng et al., Phys. Rev. **D 74**, 054507 (2006).
[16] M. Cheng et al., Phys. Rev. **D 77**, 014511 (2008).
[17] R. D. Pisarski and F. Wilczek Phys. Rev. **D 29**, 338 (1984).
[18] S. Chiku and T. Hatsuda, Phys. Rev. **D 58** 076001 (1998).
[19] T. Herpay, A. Patkós, Zs. Szép and P. Szépfalusy, Phys. Rev. **D 71** 125017 (2005).
[20] T. Herpay and Zs. Szép, Phys. Rev. **D 74** 025008 (2006).
[21] P. Kovács and Zs. Szép, Phys. Rev. **D 75** 025015 (2007).
[22] G. Fejos, A. Patkos, Phys. Rev. **D 82**, 045011 (2010); ibid **D 85**, 117502 (2012).
[23] G. Fejos arXiv:1212.3415
[24] E. S. Bowman and J. I. Kapusta, Phys. Rev. **C 79**, 015202 (2009); J. I. Kapusta, and E. S. Bowman, Nucl. Phys. **A 830**, 721C (2009).
[25] L. Ferroni, V. Koch, and M. B. Pinto, Phys. Rev. **C 82**, 055205 (2010).
[26] J. O. Andersen, R. Khan and L. T. Kyllingstad, AIP Conf. Proc. **1343** :504-506 (2011) e-Print: arXiv:1102.2779 [hep-ph]
[27] B. J. Schaefer, J. M. Pawlowski and J. Wambach, Phys. Rev. **D 76** 074023 (2007)
[28] U. S. Gupta and V. K.Tiwari, Phys. Rev. D **81**, 054019 (2010).
[29] T. K. Herbst, J. M. Pawlowski, and B.-J. Schaefer. Phys. Lett. **B 696**, 58 (2011).
[30] G. Marko and Zs. Szep, Phys. Rev.**D 82**, 065021 (2010).
[31] T. Kahara and K. Tuominen, Phys. Rev. **D 78**, 034015 (2008); ibid **D 80**, 114022 (2009). ibid **D 82**, 114026 (2010).
[32] S. Digal, E. Laermann and H. Satz, Eur. Phys. J. **C 18** 583 (2001).
[33] Claudia Ratti, Michael A. Thaler and Wolfram Weise, Phys. Rev. **D 73**, 014019 (2006).
[34] S. Rößner, C. Ratti, and W. Weise, Phys. Rev. **D 75**, 034007 (2007).
[35] H. Hansen, W. M. Alberico, A. Beraudo, A. Molinari, M. Nardi and C. Ratti, Phys. Rev. **D 75**, 065004 (2007).
[36] S. Rößner, T. Hell, C. Ratti, and W. Weise, Nucl. Phys. **A 814** 118 (2008).
[37] S. K. Ghosh, T. K. Mukherjee, M. G. Mustafa and R. Ray, Phys. Rev. **D 73**, 114007 (2006).
[38] C. Sasaki, B. Friman and K. Redlich, Phys. Rev **D 75**, 074013 (2007).
[39] T. Hell, S. Rößner, M. Cristoforetti and W. Weise, Phys. Rev **D 79**, 014022 (2009).
[40] H. Abuki, R. Anglani, R. Gatto, G. Nardulli and M. Ruggieri, Phys. Rev **D 78**, 034034 (2008).
[41] M. Ciminale, R. Gatto, N. D. Ippolito, G. Nardulli and M. Ruggieri, Phys. Rev **D 77**, 054023 (2008).
[42] W.-J. Fu, Z. Zhang and Y.-X. Liu, Phys. Rev **D 77**, 014006 (2008).
[43] K. Fukushima, Phys. Lett. **B 591** 277 (2004).
[44] K. Fukushima, Phys. Rev **D 77**, 114028 (2008).
[45] K. Fukushima, Phys. Rev **D 78**, 114019 (2008).
[46] K. Fukushima, Phys. Rev **D 79**, 074015 (2009).
[47] G. A. Contrera, M. Orsaria,and N. N. Scoccola, Phys. Rev. **D 82**, 054026 (2010).
[48] A. E. Radzhabov, D. Blaschke, M. Buballa, and M. K. Volkov, Phys. Rev. **D 83**, 116004 (2011), e-Print: arXiv:1012.0664 [hep-ph].
[49] O. Lourenco, M. Dutra, T. Frederico, A. Delfino, M. Malheiro Phys.Rev. **D 85**, 097504 (2012). O. Lourenco, M. Dutra, A. Delfino, M. Malheiro Phys.Rev. **D 84**, 125034 (2011).
[50] H. Hansen, W. M. Alberico, A. Beraudo, A Molinari, M. Nardi and C. Ratti Phys. Rev. **D 75**, 065004 (2007).
[51] P. Costa, M. C. Ruivo, C. A. de Sousa and Yu. L. Kalinovsky Phys. Rev. **D 70**, 116013 (2004).
[52] P. Costa, M. C. Ruivo, C. A. de Sousa and Yu. L.

Kalinovsky Phys. Rev. **D 71**, 116002 (2005).
[53] P. Costa, M. C. Ruivo, C. A. de Sousa, H. Hansen and W. M. Alberico Phys. Rev. **D 79**, 116003 (2009).
[54] G. A. Contrera, D. Gomez Dumm and Norberto N. Scoccola, Phys. Rev. **D 81**, 054005 (2010).
[55] B. J. Schaefer and J. Wambach, Phys. Rev. **D 75** 085015 (2007)
[56] O. Scavenius, A. Mocsy, I. N. Mishustin, D. H. Rischke, Phys. Rev. **C 64**, 045202 (2001).
[57] J. Schaffner-Bielich, Phys. Rev. Lett. **84**, 3261 (2000).
[58] J. T. Lenaghan, D. H. Rischke and J. Schaffner-Bielich, Phys. Rev **D 62**, 085008 (2000).
[59] B. J. Schaefer and M. Wagner, Phys. Rev. **D 79** 014018 (2009).
[60] G. 't Hooft, Phys. Rev. Lett. **37**, 8 (1976); Phys. Rev **D 14**, 3432 (1976).
[61] K. Fukushima, K. Ohnishi, K. Ohta, Phys. Rev **C 63**, 045203 (2001).
[62] B. J. Schaefer and M. Wagner, Prog.Part.Nucl.Phys. **62** 381 (2009)
[63] B. J. Schaefer, M. Wagner and J. Wambach, Phys. Rev. **D 81**, 074013 (2010)
[64] B. J. Schaefer, M. Wagner and J. Wambach, Proc. Sci., **CPOD2009** (2009)017.
[65] H. Mao, J. Jin and M. Huang, J. Phys. **G 37**, 035001 (2010).
[66] V. Skokov, B. Friman, E. Nakano, K. Redlich, and B.-J. Schaefer, Phys. Rev. **D 82**, 034029 (2010)
[67] A. J. Mizher, M. N. Chernodub and E. S. Fraga, Phys. Rev. **D 82**, 105016 (2010).
[68] L. F. Palhares and E. S. Fraga, Phys. Rev. D **78**, 025013 (2008) [arXiv:0803.0262 [hep-ph]].
[69] E. S. Fraga, L. F. Palhares and M. B. Pinto, Phys. Rev. D **79**, 065026 (2009) [arXiv:0902.1498 [hep-ph]].
[70] L. F. Palhares and E. S. Fraga, Phys. Rev. D **82**, 125018 (2010) [arXiv:1006.2357 [hep-ph]].
[71] U. S. Gupta and V. K.Tiwari, Phys. Rev. D **85**, 014010 (2012).
[72] B.-J. Schaefer and M. Wagner, Phys. Rev. **D 85**, 034027 (2012).
[73] Sandeep Chatterjee, Kirtimaan A. Mohan Phys.Rev. **D 85** 074018 (2012); ibid **D 86** 114021 (2012)
[74] Vivek Kumar Tiwari, Phys. Rev. D **86**, 094032 (2012).
[75] S. Weinberg Phys. Rev. **D 11**, 3583 (1975).
[76] Finite Temperature Field Theory Principles and Applications, J. I. Kapusta and C. Gale, Cambridge University Press.